ARTICLE NO. 78-204R

Shock-Wave Oscillations in a Transonic Diffuser Flow

C. P. Chen,* M. Sajben,† and J. C. Kroutil‡
McDonnell Douglas Corporation, St. Louis, Mo.

Low-frequency, self-excited oscillations involving a normal shock wave and the subsonic flow behind it were investigated experimentally in a two-dimensional diffuser. The preshock supersonic flow was uniform and steady, and the exit pressure was constant. Static wall pressure fluctuations at numerous streamwise locations were recorded and analyzed statistically for flow conditions ranging from subsonic to a shock Mach number of 1.38. Root-mean-square fluctuation intensities, power spectra, and space-time correlation maps were computed. The pressure fluctuations correlated well with the shock motion over streamwise distances comparable to the diffuser length. Both downstream-convected and upstream-propagating pressure disturbances were instrumental in sustaining the oscillations. The amplitudes of upstream-moving perturbations diminished with increasing shock strength, while the opposite was true of the downstream-moving disturbances.

Nomenclature

a = acoustic speed
A = pressure wave amplitude
C = space-time correlation
C_p = pressure coefficient, $\bar{p}/p_0$
f = frequency
h = channel height
i = $\sqrt{-1}$
K = wave number
L = streamwise length of region
M = Mach number
n = dummy index
p = pressure
q = dynamic pressure
R = amplitude ratio, A_d/A_u
S = power spectral density
t = time
U = velocity
x = streamwise coordinate
$\bar{x}$ = $(x-x_*)/h_*$
X = discrete Fourier transform
ν = overall pressure ratio, p_0/p_{atm}
ω = angular frequency, $2\pi f$
σ = normalized wave number
τ = time delay, $r\Delta t$
$\tilde{\tau}$ = $\tau f_{\max}$
ξ = x/L
ζ = ratio of measured $\hat{p}$ to inviscid prediction for (p_2-p_1)

Subscripts

0 = plenum
1 = preshock
2 = postshock
atm = atmospheric
c = core flow
d = downstream moving
max = maximum
M = midpoint of separation bubble
R = reattachment
S = separation
SH = shock
u = upstream moving
* = throat condition

Superscripts

$(\tilde{\ })$ = complex conjugate
$(\ )'$ = fluctuating component
$(\bar{\ })$ = time average
$(\hat{\ })$ = rms value

Presented as Paper 78-204 at the AIAA 16th Aerospace Sciences Meeting, Huntsville, Ala., Jan. 16-18; submitted Dec. 12, 1978; revision received April 16, 1979.

Index categories: Transonic Flow; Nozzle and Channel Flow; Nonsteady Aerodynamics.

*Research Scientist, McDonnell Douglas Research Laboratories; presently at Dynamic Technology, Inc. Member AIAA.

†Senior Scientist, McDonnell Douglas Research Laboratories. Associate Fellow AIAA.

‡Lead Engineer-Design, McDonnell Douglas Research Laboratories. Member AIAA.

Introduction

THE performance of supersonic aircraft propulsion systems is limited by the occurrence of self-excited, unsteady fluctuations in air inlets at off-design operational conditions. The purpose of the present research is to explore the properties of these fluctuations by investigating transonic flows in a two-dimensional diffuser with weak shocks near the throat. This flow contains many significant features of unsteady inlet problems, such as dynamic distortion and buzz; the flow also models unsteady, transonic processes observed in wind tunnels.

The diffuser configuration in shown in Fig. 1. The flow becomes supersonic at the throat, passes through a short supersonic zone terminated by a shock in the divergent section, and continues to decelerate subsonically to the model exit. The Reynolds number based on throat height is approximately 1×10^6 and the greatest time-mean Mach number in the flow is approximately 1.4. The subsonic region contains rapidly growing boundary layers and a separation bubble on the upper wall at all transonic conditions. Flow is steady upstream of the shock, but the shock and the entire subsonic zone display large-amplitude, low-frequency fluctuations.

Previous work on this and similar models[1,2] has described the qualitative appearance of the flows as seen in high-speed movies, the time-mean surface pressure distributions, separation, and reattachment locations, and a time-mean and statistical characterization of the shock motion. Five qualitatively different transonic flow modes have been identified and described. A summary of these results is given in Figs. 2 and 3.

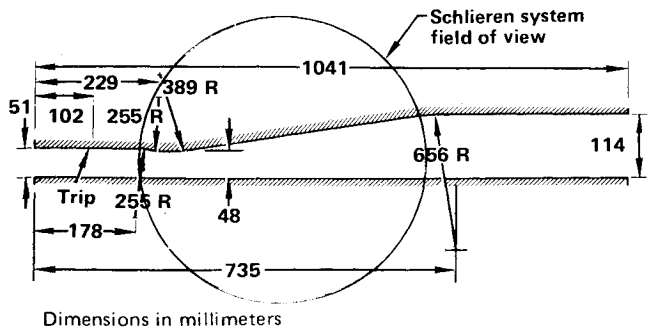

Fig. 1 Diffuser model contours. (Spanwise dimension of channel = 152 mm; trip size = 0.51 mm in both vertical and streamwise directions; bottom slot inclination = 30 deg; slot opening = 0.51 mm.)

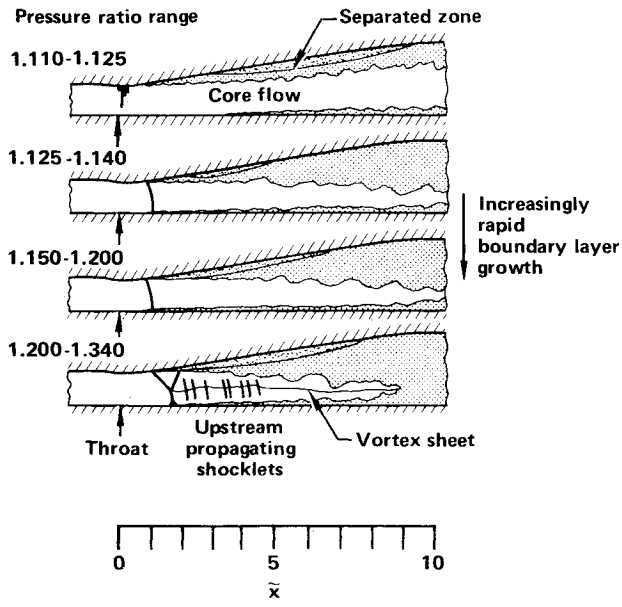

Fig. 2 Typical instantaneous flow patterns.

The only basic experimental study of fluctuating, transonic channel flow known to the authors is that of Meier,[3] who found a nearly periodic flow, alternately displaying shock- and pressure-gradient induced separation, and shock propagation through the throat.

Much useful, related information is contained in studies dealing with wall pressure fluctuations in the framework of low-speed boundary layer turbulence. A survey of this topic is given by Willmarth.[4]

Published wall pressure fluctuation measurements in unsteady transonic and supersonic flows were mostly directed toward understanding buffet in airfoil and wing flows.[5,6] Roos and Riddle[7] made extensive dynamic wall pressure measurements in a supercritical airfoil flowfield displaying shock oscillations. Our findings have many parallels and similarities to theirs, despite the major differences in the configuration of solid boundaries.

The present work utilizes time-dependent pressure measurements along the flat, bottom wall of the diffuser model to gain insight into the nature of the unsteady oscillations observed. Thirteen miniature, high-response, flush-mounted pressure transducers provided sufficient resolution in time and space for detailed statistical analysis. Root-mean-square fluctuation intensities, probability density functions (PDF), and power spectral densities (PSD) were computed for the fluctuating components of all signals, and space-time correlations (STC) were determined for selected signal pairs. The results are examined and interpreted in terms of fluid mechanical processes.

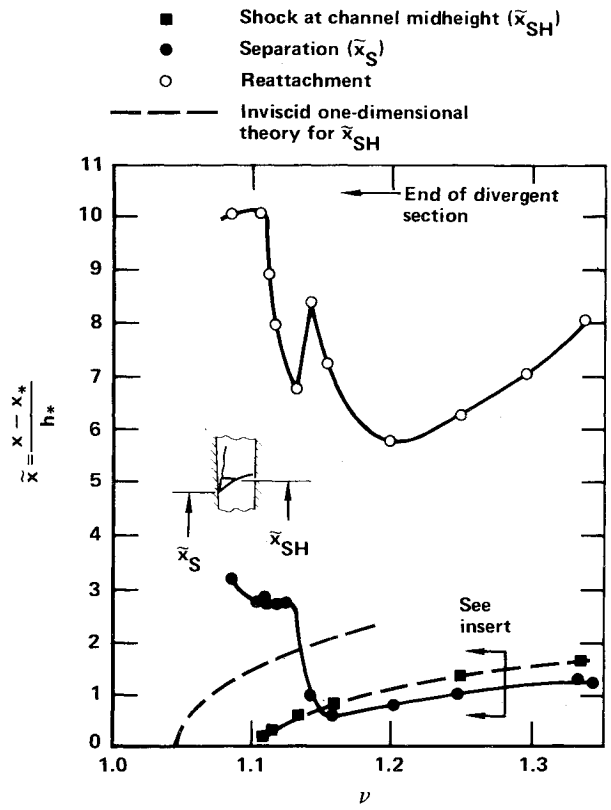

Fig. 3 Separation and reattachment locations for top wall; also shock positions in mid-channel. (Insert illustrates why $\tilde{x}_{SH} \gg \tilde{x}_S$ for $\nu \gg 1.15$.)

Equipment and Experimental Procedures

Diffuser Model

The diffuser model has an exit-to-throat area ratio of 2.37 and a maximum divergence angle of 8.8 deg. Layout and principle dimensions are shown in Fig. 1.

The model was attached to a plenum chamber with a 25:1 contraction immediately upstream of the model. A square-wave-shaped, spanwise insert with 0.51-mm tooth height tripped the boundary layer on the top wall; the bottom-wall boundary layer was removed through a suction slot at the same streamwise location as the trip. Additional suction was applied on the approach section side walls as well as along the top-wall/side-wall corners to remove low-energy boundary-layer fluid. The resultant mean flowfield was satisfactorily two-dimensional.[2]

The glass side-walls of the divergent section allowed the use of Schlieren and shadowgraph flow-visualization techniques. The flow exhausted to the ambient atmosphere through a constant-area segment, as shown in Fig. 1.

The only variable parameter was the plenum total pressure p_0. The pressure ratio ν, defined as the ratio of plenum total pressure to atmospheric exit (static) pressure, was used to characterize test conditions.

Instrumentation

Miniature, 2-mm-diam strain gage-type transducers (Kulite model CQL-080) were used to measure fluctuating pressures on the bottom wall. These transducers have a linear dynamic range of ± 175 kPa and a flat frequency response to 90 kHz.

Inside the oscillating range of the shock-wave, transducers were densely spaced (6.4-mm apart) and staggered in the spanwise direction to reduce mutual interference; further downstream they were separated by increasing streamwise distances. Fluctuating pressure signals were recorded on a 14-track FM tape recorder (Sangamo Sabre III), digitized at 4 kHz with 15 bit accuracy, and processed by computer. Analog

signals were low-passed before digitization by a third-order Butterworth filter with a 1 kHz cutoff frequency. Unfiltered spectra showed this frequency range to be more than adequate.

A simultaneous, high-speed Schlieren film at 44,000 frames/s was taken during each run. The tape recorder and the movie cameras were synchronized by appropriate optical/electronic marker signals.

Digital Processing of Signals

All statistical information in this paper was computed from 18.75 s duration records, corresponding to 75,000 digital points from each pressure transducer. Mean pressure and fluctuating pressure levels were computed as

$$\bar{p}(\bar{x}) = \frac{1}{N} \sum_{n=0}^{N-1} p(\bar{x}, n\Delta t) \tag{1}$$

and

$$\hat{p}(\bar{x}) = \left\{ \frac{1}{N} \sum_{n=0}^{N-1} \left[p(\bar{x}, n\Delta t) - \bar{p}(\bar{x}) \right]^2 \right\}^{1/2} \tag{2}$$

where $N=75{,}000$ and Δt is the digitizing interval (0.25 ms). The Cooley-Tukey fast-Fourier transform algorithm was used to calculate power spectral densities and correlations of pressure signals. For the former application, a set of 512 points was tapered by a cosine window to reduce spectral leakage and was subsequently Fourier-transformed.[8] The frequency resolution and the bandwidth of this spectral density are 7.8 Hz and 2000 Hz, respectively. Mathematically, the discrete Fourier transform of the pressure fluctuation is

$$X_K = \frac{1}{N} \sum_{n=0}^{N-1} \left[p(\bar{x}, n\Delta t) - \bar{p}(\bar{x}) \right] \exp\left[-i \frac{2\pi K n}{N} \right] \tag{3}$$

where $K=0,1,\ldots, N/2-1$ and $N=512$. The spectral density S_K is the amplitude of each spectral component:

$$S_K = X_K \cdot \tilde{X}_K \tag{4}$$

where $\tilde{X}_K$ is the complex conjugate of X_K. The power spectral density presented is the average of 146 sets of spectral amplitudes.

The normalized space-time correlation between pressure signals from two different locations x_a, x_b is defined as

$$C(\bar{x}_a, \bar{x}_b, \tau) = \left\{ \sum_{n=0}^{N-r-1} \left[p(\bar{x}_a, n\Delta t) - \bar{p}(\bar{x}_a) \right] \times \left[p(x_b, n\Delta t + r\Delta t) - p(\bar{x}_b) \right] \right\} \Big/ (N-r)\hat{p}(\bar{x}_a)\hat{p}(\bar{x}_b) \tag{5}$$

When $\bar{x}_a = \bar{x}_b$, Eq. (5) yields the autocorrelation. The method of Ref. 9 was used in the computations.

Results and Discussion

Visual Observations

Schlieren films showed the bottom-wall boundary layer to be thin compared with that on the top wall, for all streamwise locations and pressure ratios. At the downstream end of the diffuser, the bottom-wall displacement thickness was ~4 mm, the core flow speed was ~80 m/s, and fluctuations associated with boundary turbulence occurred from 3 to 20 kHz. These fluctuations, representing a small fraction of the total energy, were filtered out and did not influence the recorded wall pressure signals significantly. The signals thus reflect core flow static pressures prevailing at the outer edge of the bottom-wall boundary layer.

The unsteady part of the core flow pressure was governed primarily by the separated, rapidly growing top-wall boundary layer whose displacement thickness distribution was modulated strongly by the oscillations. The typical time-mean thickness at the diffuser exit was ~20 mm. Two different kinds of modulation were found, having different origins and frequency ranges.

One type of modulation was related to the corrugations on the boundary-layer/core-flow interface, created by the large eddy structures within the layer. The streamwise eddy spacing varied from 20 to 100 mm and was expected to cause fluctuations from 1.0 to 4.0 kHz. These fluctuations were present, but their energy was only a minor part of the total and was eliminated from the pressure data by filtering. Pressure fluctuations of this type were directly observable in the Schlieren films[2] for $\nu \geq 1.25$ as trains of weak but distinct shocklets, moving upstream in the core flow with an irregular streamwise spacing of 30-60 mm and with a speed approximating $(a - U_c)$.

The second type of modulation of the top-wall layer occurred at frequencies comparable to shock displacement variations (0-300 Hz) and wavelengths comparable to, or possibly greater than, the diffuser length. Since the field-of-view of the Schlieren system included less than half of the diffuser, spark photographs show only a fraction of a wave and do not yield clear evidence of their presence. However, the quantitative analysis of pressure perturbations presented here indicates that this type of fluctuation contained the bulk of fluctuation energy.

Time-Mean Flow

Detailed measurements were made at seven different pressure ratios; a summary of the flow characteristics is given in Table 1 and in Figs. 2 and 3. The time-mean surface pressure distributions measured on the bottom wall are given in Fig. 4.

All bottom-wall pressure distributions are remarkably similar to the top-wall pressure distributions,[1,2] showing the absence of large vertical pressure gradients. Significant differences occur within only one or two throat heights from the throat location where wall curvature and shock-boundary layer interaction effects are important.

Oil flow traces and Schlieren photographs indicate that the bottom-wall layer is always thin and unseparated; if separation does occur, the bubble is too small to be detected by oil flow methods. It is thus not surprising that the pressure distributions on both walls are related to the behavior of the top-wall boundary layer only. If separation is caused by an adverse pressure gradient ($\nu \leq 1.13$), then the $\bar{p}(\bar{x})$ for either wall shows no apparent anomalies. In contrast, shock-induced separation creates a break in the distributions, followed by a short plateau. The plateaus are especially pronounced if the shock displays a definite lambda pattern, as is the case for $\nu = 1.25$ and 1.34 in Fig. 4.

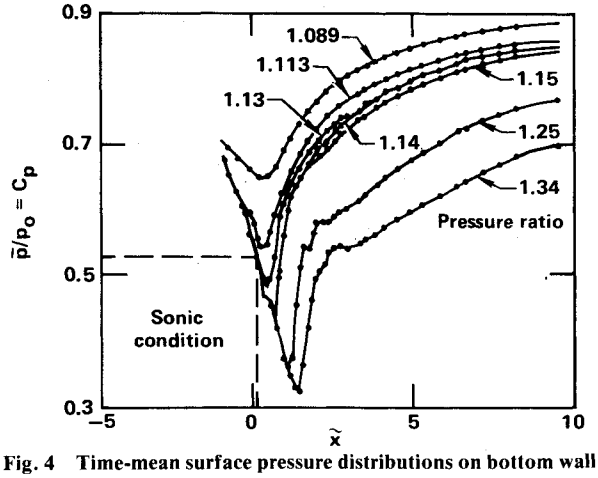

Fig. 4 Time-mean surface pressure distributions on bottom wall.

Table 1 Summary of flow characteristics

Pressure ratio ν	Supersonic region	Shock	Shock geometry	Separation induced by
1.089	nonexistent	nonexistent	—	—
1.112	intermittent	intermittent	multiple, normal	adverse pressure gradient
1.13	persistent	persistent	single, normal	adverse pressure gradient
1.14	persistent	persistent	single, normal	and shock (alternately)
1.15	persistent	persistent	single, normal	
1.25	persistent	persistent	single, lambda	shock
1.34	persistent	persistent	single, lambda	

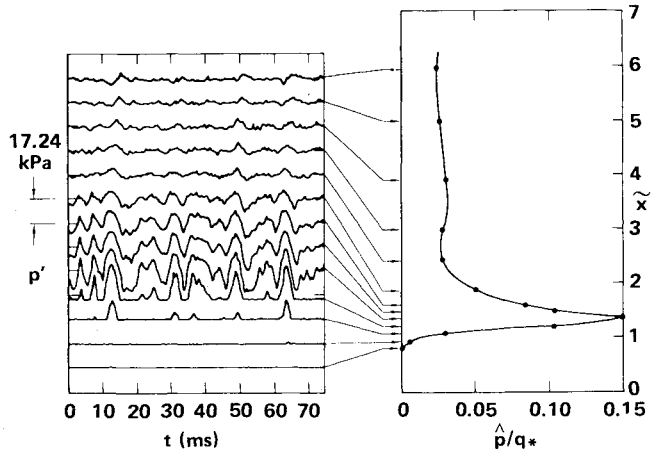

Fig. 5 Wall pressure fluctuations for $\nu = 1.25$. (Left side shows fluctuating components of transducer signals; right side is streamwise distribution of normalized rms values.)

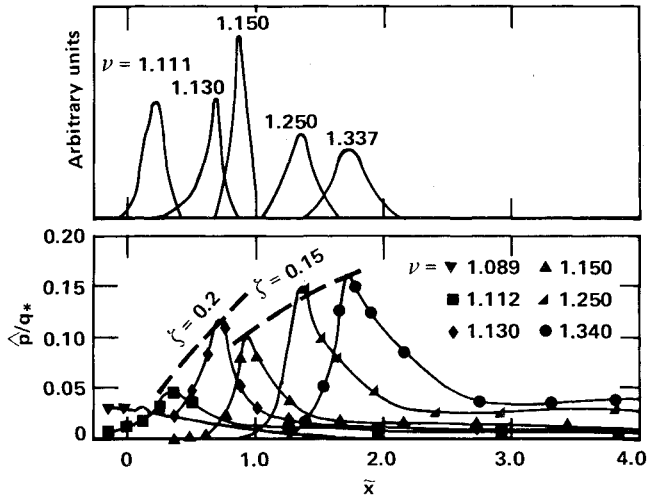

Fig. 6 Distributions of probability density for shock position (top) and rms wall pressure fluctuation intensity (bottom). (Dashed lines represent ζ times the pressure difference across a stationary, normal shock at $\tilde{x}$.)

Simultaneous Pressure Histories

Figure 5 shows a sample of 13 simultaneous pressure histories at $\nu = 1.25$, corresponding to shock-induced separation. Within the shock oscillation range, the pressure signals are reminiscent of square waves, as expected, although the fluctuations present during the "on" portion of the wave (subsonic flow over the transducer) are of considerable magnitude.

The repetition of like patterns at adjacent stations with small time shifts presage high correlations in the streamwise direction. The pattern similarities clearly connect the shock motion with the weaker pressure waves further downstream.

Similar features of pressure signals were observed at all flow conditions.

Fluctuating Pressure (rms) Intensities

The streamwise distribution of the fluctuating pressure (rms) levels is shown in Fig. 6 for six pressure ratios, together with probability density distributions for shock position.[2]

For the subsonic case ($\nu = 1.089$), $\hat{p}/q_*$ is highest at the throat and decreases monotonically downstream. The high value near the throat may be related to the steepening of compression waves arriving from downstream.[10]

All supercritical cases show the expected qualitative appearance: negligible fluctuations before the shock, a pronounced peak, and a relatively high, nearly constant level in the downstream, subsonic region.

Within the range of peak $\hat{p}$ values, the signals are dominated by the passage of the shock over the transducers. The shock displacement amplitudes define the width of the $\hat{p}$ peak, and the maximum values of $\hat{p}$ are proportional to the theoretical pressure differential across a stationary normal shock at the measured mean shock location ($\equiv \Delta p_{SH}$). The measured $\hat{p}_{max}$ is approximately 20% of Δp_{SH} for pressure-gradient-induced separation and 15% for shock-induced separation; both are comparable to the 16.7% expected for Gaussian signals. Figure 6 illustrates the trend by showing the quantity $\zeta \Delta p_{SH}/q_*$ as a function of the shock position with $\zeta = 0.15$ and 0.2.

The $\hat{p}$ peaks are followed by plateaus of lesser but still considerable magnitude, downstream of the oscillating range of the shock. Knowing the time history of shock position, it is possible to obtain inviscid estimates of the pressure fluctuations in the subsonic flow. The measured $\hat{p}$ values are well over such estimates even for weak shocks and are much above them if the separation is shock induced ($\nu = 1.25$ and 1.35 in Fig. 6). The large measured rms values are, however, not unexpected in view of the violent unsteadiness observed in Schlieren films.

Power Spectral Densities

Figure 7 shows power spectral densities at various pressure ratios. Each was taken at the location of the respective $\hat{p}_{max}$ and is normalized by this value. For this reason, spectral densities for any given frequency are not comparable directly among various stations. The spectra of Fig. 7 are similar to those for shock displacements obtained by independent methods and presented elsewhere.[2]

There is significant spectral density below approximately 70 Hz at pressure ratios ≤ 1.13, which corresponds to flows with pressure-gradient-induced separation. This low-frequency contribution was also observed on shock position spectra and may be related to a slow drifting of the separation point, whose location does not coincide with the position of the shock. In cases with shock-induced separation, the separation point location rigorously coincides with the shock, whose motion in such a situation does not contain extremely low frequencies.

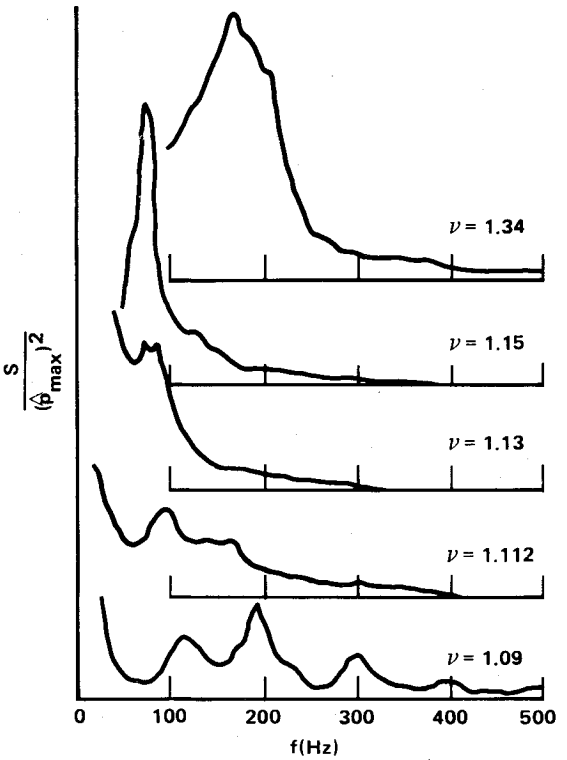

Fig. 7 Power spectral density of fluctuating pressure signals at the mean shock position.

The subsonic flow shows four distinct peaks, at 115, 195, 295, and 395 Hz. Even though the last three peaks are not exact multiples of the first, they are close enough to be regarded as harmonics. An estimate of the fundamental frequency of the open duct, taking into account the flow speed, is 110 Hz, suggesting that the pressure disturbances in the core flow can be attributed to standing waves. In contrast, all supercritical spectra display a single peak which appears to evolve from the fundamental harmonic of the high subsonic case. As ν increases, the peak gradually moves to lower frequencies and gradually becomes narrower. At $\nu = 1.15$, the sharp peak indicates a nearly periodic flow with 70 Hz frequency. $\nu = 1.15$ represents a transitional case between pressure-gradient and shock-induced separations, and most likely involves an intermittent coincidence of shock and separation point locations. In this respect, our flow at $\nu = 1.15$ is similar to that described by Meier.[3]

Further increases of ν result in the reversal of both tendencies: the peak frequency rises rapidly while the spectrum becomes quite broad. Minor peaks appear over 1 kHz in unfiltered spectra (not shown), which are thought to be related to upstream-propagating weak shocklets, readily observable in high-speed films.

The streamwise evolution of the PSDs reveals features dependent on whether the separation is induced by the pressure gradient or by the shock.

Figure 8 demonstrates PSDs at several streamwise locations under conditions of pressure-gradient-induced separation ($\nu = 1.112$). The primary peak at the dominant shock oscillation frequency (94 Hz) is clearly present at all locations as is the low-frequency contribution. Minor broad peaks may be found over 100 Hz and may be related to the clustered, multiple structure of the shock at $\tilde{x} = 0.26$ and to large-scale turbulence in the separation bubble at $\tilde{x} = 3.82$ and 5.79.

Figure 9 shows the even simpler pattern of the shock-induced separation ($\nu = 1.34$). The shock oscillations dominate the fluctuations everywhere; the spectral peak at all locations occurs at the same frequency, which agrees with the dominant frequency taken from shock position spectra. Some

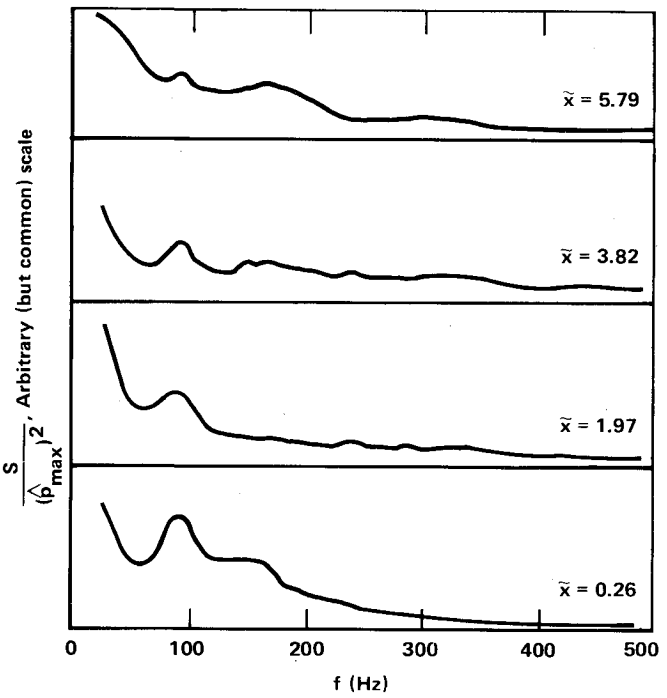

Fig. 8 Streamwise evolution of power spectra for fluctuating pressure at $\nu = 1.112$.

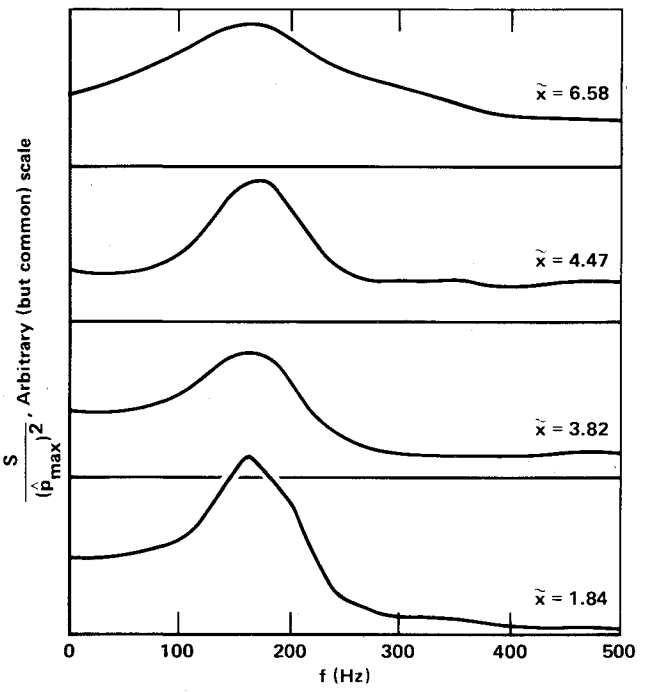

Fig. 9 Streamwise evolution of power spectra for fluctuating pressure at $\nu = 1.34$.

broadening occurs downstream, indicating the development of smaller eddies in the flow.

Intermediate cases ($\nu \approx 1.13$ to 1.15) result in complex PSDs with dual peaks whose interpretation is not attempted here.

Space-Time Correlations

The procedure in computing STCs was to select the transducer signal closest to the time-mean shock-position as reference and correlate it with itself and the remaining 12 signals. The aggregate of the computed 13 correlations was displayed on a time-delay vs streamwise location plane, using contour lines having constant values of the correlation

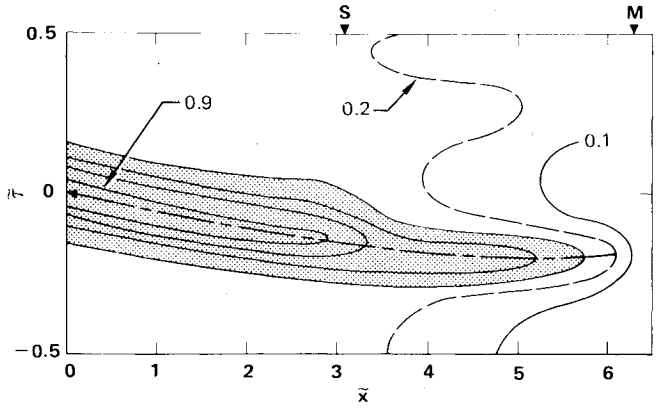

Fig. 10 Contour map of space-time correlation coefficients (C) for $\nu = 1.09$. Time delay scale normalized by $1/f_{max} = 8.7$ ms. Top portion shows separation point (S), and midpoint of separation bubble (M). Increment of C between adjacent solid lines is 0.2; intermediate values are shown as dashed lines. Shaded areas emphasize positive values of C.

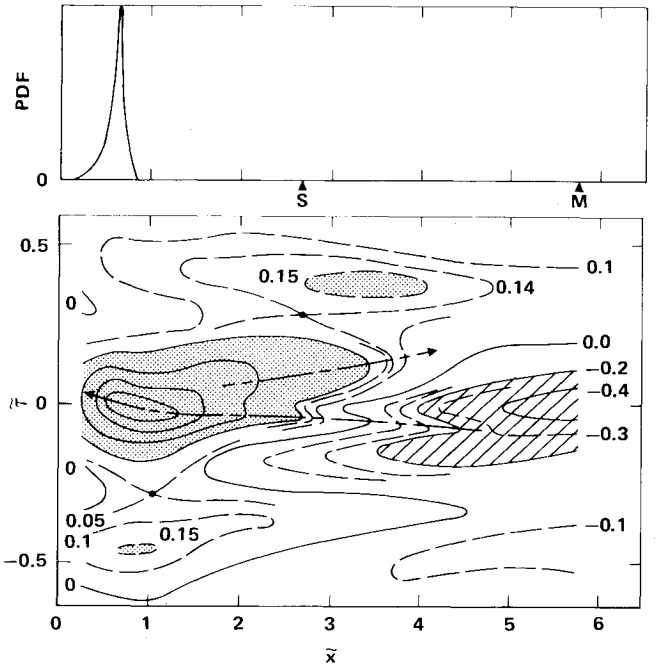

Fig. 11 Contour map of space-time correlation coefficients (C) for $\nu = 1.13$. Time delay scale normalized by $1/f_{max} = 12.5$ ms. Top portion shows shock position PDF, separation point (S), and midpoint of separation bubble (M). Increment of C between adjacent solid lines is 0.2; intermediate values are shown as dashed lines. Shaded and cross-hatched areas emphasize positive and negative values of C, respectively.

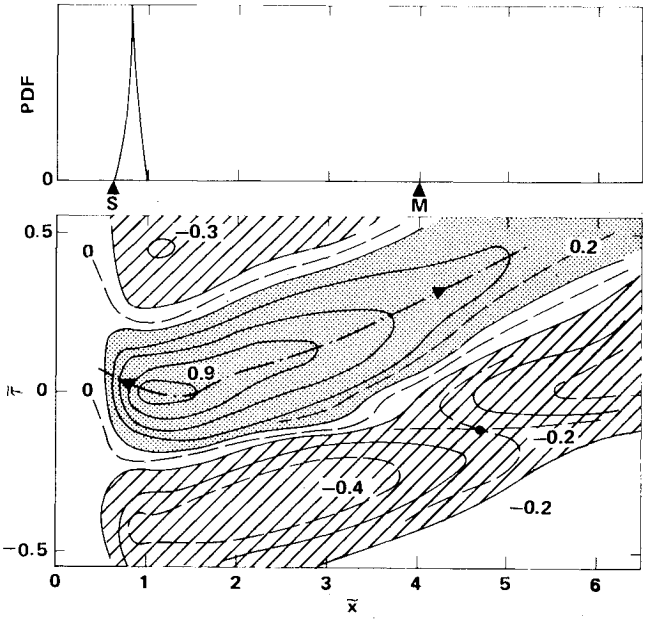

Fig. 12 Contour map of space-time correlation coefficients (C) for $\nu = 1.15$. Time delay scale normalized by $1/f_{max} = 14.3$ ms. Top portion shows shock position PDF, separation point (S), and midpoint of separation bubble (M). Increment of C between adjacent solid lines is 0.2; intermediate values are shown as dashed lines. Shaded and cross-hatched areas emphasize positive and negative values of C, respectively.

coefficient. This representation is reminiscent of an x-t diagram describing the behavior of a typical oscillatory event: lines with negative (positive) slope correspond to upstream (downstream) moving perturbations.

To illustrate the relationship of STCs to the power spectra of the reference signal, the time-delay scale is made dimensionless by the frequency at which the spectral peak occurs (f_{max}, taken from Fig. 7). For comparison, the PDF for shock position and the time-mean separation point are shown on the contour maps. Since the reattachment point is beyond the x range of the plots, the midpoint of the separation bubble ($1/2\ (\tilde{x}_S + \tilde{x}_R) = \tilde{x}_M$) is marked on each contour map as a reference.

Figure 10 ($\nu = 1.09$) describes subcritical flow, i.e., subsonic flow without shocks. The dominant feature is an elongated cluster of contour lines, corresponding to a sequence of peaks on the individual correlation curves. In terms of map features, this sequence of peaks is a locus of points where the contour lines have a vertical slope. If the contour map is thought of as a three-dimensional surface, then the locus defines a ridge-shaped topological feature and will be referred to as a ridge in this paper. The inverse of the ridge slope on the $(\tilde{\tau}, \tilde{x})$ plane is commonly interpreted in experimental practice as the propagation (or convection) speed of the perturbations. The ridge of Fig. 10 indicates a single, upstream-moving family of perturbations whose speed is approximately $(a - U)$. There is no evidence of downstream-moving disturbances.

Figure 11 corresponds to a situation ($\nu = 1.13$) in which shock-induced separation probably occurs intermittently, alternating randomly with pressure-gradient-induced separation. The correlation map reflects the complexity of this intermediate situation.

Figures 12 and 13 describe supercritical flows with shock-induced separation, at two different shock strengths. Both maps are distinctly repetitive with a nondimensional period of unity, thus reflecting events that occur at the dominant frequency f_{max}.

Within the oscillating range of the shock, where the pressure signals are dominated by the shock passage over the sensors, all correlation contours show a negative slope, i.e., upstream motion of disturbances. This observation can be related to the evidence (from Schlieren films) that the upstream motion of the shock seems to follow nearly the same x-t trajectory each time and that the shock is strong while moving upstream. In contrast, downstream movements of the shock tend to be associated with lower strengths and are more random in character. The statistical processing of the corresponding position histories results in a clear indication of upstream movement, while downstream displacements average to insignificant correlation coefficients.

Outside the shock oscillation range, the ridges in Figs. 12 and 13 have positive slopes, indicating that the downstream motion of perturbations dominates the supercritical cases. This trend is emphasized by shading areas of positive or negative C differently. The speed suggested by the slope of the

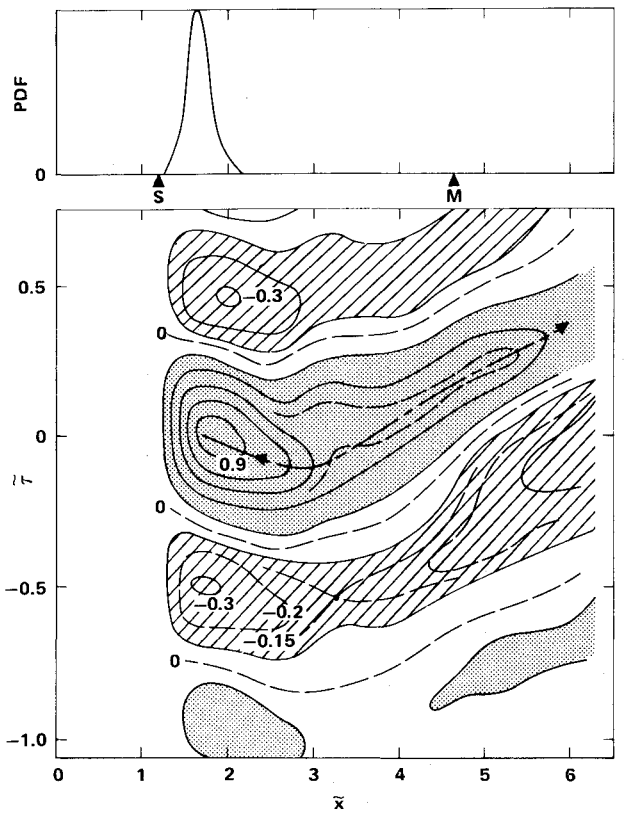

Fig. 13 Contour map of space-time correlation coefficients (C) for $\nu = 1.34$. Time-delay scale normalized by $1/f_{max} = 6.0$ ms. Top portion shows shock position PDF, separation point (S), and midpoint of separation bubble (M). Increment of C between adjacent solid lines is 0.2; intermediate values are shown as dashed lines. Shaded and cross-hatched areas emphasize positive and negative values of C, respectively.

shaded strips ranges from 30 to 70 m/s; in all cases it is well below the core flow velocity and negligible compared with the speed of downstream propagating pressure waves. The only reasonable explanation is that the perturbations are convected within the boundary layer, largely on the top wall. The perturbations are immediately communicated to (and somewhat modified by) the core flow and are, therefore, detectable on the bottom wall. The entire process is well correlated with the wall pressure at the mean shock position, and thereby also with the shock motion.

Upstream-propagating disturbances are weak in cases of shock-induced separation, but they are detectable as spatially coherent sequences of repetitive contour-line features. At $\nu = 1.13$ (intermittent occurrence of shock-induced separation), a ridge associated with upstream movement is clearly defined and is shown by a dashed line. At $\nu = 1.15$ an array of inflection points is initiated at the reference point (where $C = 1$) and terminated at a saddle point. (Saddle points are crossings of contour lines. Some comments on their significance will be made in the next section.) At $\nu = 1.34$, in the presence of strong shock-induced separation, strong convection effects severely mask the features of upstream-moving perturbations, but a saddle point is still clearly present.

In summary, the space-time correlations conclusively indicate the presence of two types of moving disturbances: one convected downstream and one propagating upstream. Both are highly correlated with the motion of the shock. The relative amplitudes of the two are reversed as the pressure ratio changes over the experimental range; upstream propagation dominates the highly subsonic case, but quickly becomes a secondary contributor as shock strength increases,

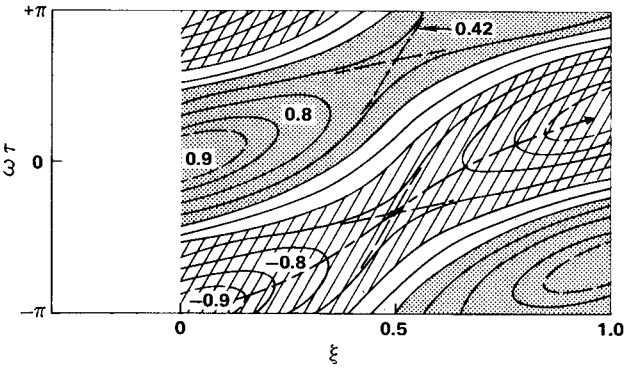

Fig. 14 Synthesized correlation map for $\sigma_u = 4\pi/3$, $n = 2$ and $R = 2.5$.

and is almost completely masked by convective perturbations at $\nu = 1.34$.

Synthesized Perturbation Patterns

The statistical, indirect evidence of space-time correlations suggests the physical picture of two families of superimposed, one-dimensional perturbations of unequal speeds and amplitudes moving in opposite directions. Such patterns can be hypothesized in mathematical terms, and determination of the corresponding correlations is straightforward. If the hypothesized pattern is a good approximation of the individual events occurring in reality, then the STCs deduced from the hypothesis should resemble closely the experimentally obtained maps (Figs. 11-13). Using the procedure described below, close similarity was found.

For simplicity, both families of perturbations are assumed to be wave-like, despite the fact that one family is known to be a convective phenomenon. Neglecting the streamwise deceleration of the flow, both phase velocities are considered constants, with numerical values specified to approximate experimental data.

The two families are connected via boundary conditions at both ends; these boundary conditions specify how an incoming wave of one type is reflected as an outgoing wave of another type. The physical complexity of the reflection process is not considered; the outgoing wave amplitude at the upstream end is assumed equal to R times the arriving wave amplitude. A similar condition is imposed at the downstream end; consistency requires that the ratio of reflected and incoming amplitudes at this point be $1/R$. The mathematical expression for the perturbation field is then

$$P(x,t) \equiv \frac{p'_d + p'_u}{A_u} = R\sin(\omega t - \sigma_d \xi) + \sin(\omega t + \sigma_u \xi) \qquad (6)$$

The boundary conditions will be satisfied if the following relation holds:

$$\sigma_d + \sigma_u = n\pi \qquad (7)$$

where n is an even integer. Using the analytical equivalent of Eq. (5), the space-time correlation is

$$C(0,\xi,\omega\tau) = \frac{1}{R+1}\left[R\cos\sigma_d\xi + \cos(n\pi - \sigma_d)\xi\right]\cos\omega\tau + \left[R\sin\sigma_d\xi - \sin(n\pi - \sigma_d)\xi\right]\sin\omega\tau \qquad (8)$$

This expression contains the arbitrary constants, R, σ_d, and n, whose values were chosen (after some trial and error) to be 2.5, $4\pi/3$, and 2, respectively. These values imply that the downstream-moving perturbations have larger amplitudes and slower speeds than the upstream-moving perturbations, a situation typical of flows with shock-induced separation.

Despite the gross simplification made, the similarity between the calculated correlation map of Fig. 14 and the experimental map of Fig. 12 is striking. Both maps display the inclined clusters of contours depicting the downstream movement. The weaker and faster upstream perturbations are not reflected explicitly in Fig. 14, but they do give rise to a saddle point. This finding justifies the interpretation of the saddle point in Fig. 12 as an indication of the presence of weak, upstream-moving perturbations. The fact that some of the experimental data (Fig. 11) show upstream waves more lucidly than Fig. 14 suggests that real waves may be concentrated in sharper fronts than the sine wave used in the model.

The calculations of this section do not consitute a theory, but they do illustrate that counter-running wave-trains of unequal amplitude and speed are compatible with the experimental data.

Summary

Transonic diffuser flows displaying self-excited fluctuations were investigated by subjecting time-dependent surface static pressure data to a classical statistical analysis.

The analysis shows that the bulk of the fluctuation energy is contained in the frequency range of the shock oscillations, i.e., below approximately 300 Hz. Fluctuations associated with turbulence in the separated top-wall boundary layer represent minor contributions, and effects of the attached bottom-wall layer on the signals are negligible. The fluctuations are highly correlated over streamwise distances comparable to the diffuser length.

The oscillations are associated with two types of pressure disturbances: one is related to pressure waves propagating upstream in the core flow, and the second is convected downstream, mostly carried by the top-wall boundary layer. The relative amplitudes associated with the convective disturbances increase with shock strength; the opposite is true for the upstream-moving waves.

The character of the fluctuations is dependent on the immediate cause of separation. For weak shocks ($M_{SH} \ll 1.3$), separation is induced by the adverse pressure gradient in the divergent section. In this range the peak oscillation frequency decreases with shock strength, and there is a significant spectral content at low frequencies.

For strong shocks ($M_{SH} \gg 1.3$), separation occurs at the shock foot. There is no appreciable fluctuation energy below the shock motion frequency; peak frequencies and shock oscillation amplitudes both increase with shock strength.

The observations are consistent with a model postulating two families of perturbations coexisting in a region lying between the shock and the reattachment point and both behaving as waves. Upstream-moving waves are fast and weak, while downstream-moving waves are slow and strong. If all waves are assumed to reflect in like sense at both ends, then the calculated correlation maps show a striking resemblance to experimental data.

Acknowledgment

This research was conducted under the McDonnell Douglas Independent Research and Development Program.

References

[1]Sajben, M., Kroutil, J.C., and Chen, C.P., "A High-Speed Schlieren Investigation of Diffuser Flows with Dynamic Distortion," AIAA Paper 77-875, July 1977.

[2]Sajben, M., Kroutil, J.C., and Chen, C.P., "Unsteady Transonic Flow in a Two-Dimensional Diffuser," *AGARD Conference Proceedings on Unsteady Aerodynamics*, No. 227, 1977.

[3]Meier, G.E.A., "Shock Induced Flow Oscillations," *AGARD Proceedings on Flow Separation*, No. 168, 1974.

[4]Willmarth, W.W., "Pressure Fluctuations Beneath Turbulent Boundary Layers," *Annual Review of Fluid Mechanics*, Vol. 7, Annual Reviews Inc., Palo Alto, Calif., 1975, pp. 13-38.

[5]Kistler, A.L., "Fluctuating Wall Pressure Under A Separated Supersonic Flow," *Journal of the Acoustical Society of America*, Vol. 36, March 1964, pp. 548-550.

[6]Speaker, W.B. and Ailman, C.M., "Static and Fluctuation Pressure in Regions of Separated Flow," AIAA Paper 76-66, Jan. 1976.

[7]Roos, F.W. and Riddle, D.W., "Measurement of Surface Pressure and Wake Flow Fluctuations in the Flow Field of a Whitcomb Supercritical Airfoil," NASA TN D-8443, Aug. 1977.

[8]Gingham, C., Godfrey, M.D., and Tukey, J.W., "Modern Techniques of Power Spectrum Estimation," *Audio and Electroacoustics*, Vol. AU-15, June 1967, pp. 56-66.

[9]Otnes, R.K. and Enochson, L., *Digital Time Series Analysis*, Wiley-Intersciences, New York, 1972, p. 247.

[10]Shapiro, A.H., *Compressible Fluid Flow*, Vol. II, The Ronald Press Co., New York, 1954, Chap. 23.